



## OPEN

## Fullerene mixing effect on carrier formation in bulk-hetero organic solar cell

## SUBJECT AREAS:

SOLAR CELLS  
LIGHT HARVESTING  
POLYMERSReceived  
17 November 2014Accepted  
6 March 2015Published  
30 March 2015Correspondence and  
requests for materials  
should be addressed to  
Y.M. (moritomo.  
yutaka.gf@u.tsukuba.  
ac.jp)Yutaka Moritomo<sup>1,2</sup>, Takeshi Yasuda<sup>3</sup>, Kouhei Yonezawa<sup>1</sup>, Takeaki Sakurai<sup>1,4</sup>, Yasuo Takeichi<sup>5</sup>, Hiroki Suga<sup>6</sup>, Yoshio Takahashi<sup>5,7</sup>, Nobuyuki Inami<sup>5</sup>, Kazuhiko Mase<sup>5</sup> & Kanta Ono<sup>5</sup>

<sup>1</sup>Faculty of Pure and Applied Science, Univ. of Tsukuba, Tsukuba 305-8571, Japan, <sup>2</sup>Center for Integrated Research in Fundamental Science and Engineering (CiRFSE), Univ. of Tsukuba, Tsukuba 305-8571, Japan, <sup>3</sup>Photovoltaic Materials Unit, National Institute for Materials Science (NIMS), Tsukuba, Ibaraki 305-0047, Japan, <sup>4</sup>PRESTO, Japan Science and Technology Agency, Saitama 332-0012, Japan, <sup>5</sup>Institute of Materials Structure Science, High-Energy Accelerator Research Organization (KEK), Tsukuba, Ibaraki 305-0801, Japan, <sup>6</sup>Department of Earth and Planetary Systems Science, Hiroshima University, Higashi-hiroshima, Hiroshima 739-8526, Japan, <sup>7</sup>Department of Earth and Planetary Science, Univ. of Tokyo, Bunkyo-ku, Tokyo 113-0033, Japan.

Organic solar cells (OSCs) with a bulk-heterojunction (BHJ) are promising energy conversion devices, because they are flexible and environmental-friendly, and can be fabricated by low-cost roll-to-roll process. Here, we systematically investigated the interrelations between photovoltaic properties and the domain morphology of the active layer in OSCs based on films of poly-(9,9-dioctylfluorene-co-bithiophene) (F8T2)/[6,6]-phenyl C<sub>71</sub>-butyric acid methyl ester (PC<sub>71</sub>BM) blend annealed at various temperatures ( $T_{an}$ ). The scanning transmission X-ray microscopy (STXM) revealed that fullerene mixing ( $\Phi_{Fullerene}$ ) in the polymer matrix decreases with increase in  $T_{an}$  while the domain size ( $L$ ) is nearly independent of  $T_{an}$ . The TEM-S mapping image suggests that the polymer matrix consist of polymer clusters of several nm and fullerene. We found that the charge formation efficiency ( $\Phi_{CF}$ ), internal quantum efficiency ( $\Phi_{IQ}$ ), and power conversion efficiency (PCE) are dominantly determined by  $\Phi_{Fullerene}$ . We interpreted these observations in terms of the polymer clusters within the polymer matrix.

In OSCs, the light-to-electric energy conversion is realized by the combination of the carrier formation and transfer processes within the active layer (Fig. S1). In the former process, the photo irradiation creates a donor exciton in the donor region and the donor exciton migrates to the donor (D)/acceptor (A) interface. Finally, the exciton separates into the electron and hole at the D/A interface. In most cases, the electron and hole are weakly bound to each other around the interface. In the latter process, the carriers transfer to the collector electrode and are collected as photocurrent. This is in a sharp contrast with an inorganic solar cell (ISC), in which the photo-irradiation directly creates carriers within the active layer.

The BHJ active layer of OSC consists of phase-separated nano-size (several tens of nm) domains of the donor polymer and acceptor fullerene<sup>1–5</sup>. The nano-size structure is essential for the efficient carrier formation process, because the length of exciton migration is  $\sim 3$  nm. The STXM around the carbon K-edge is a powerful tool to clarify the molecular mixing as well as the domain structure in the BHJ active layer<sup>6,7</sup>, because it can distinguish the fullerene carbon from the polymer carbon. For example, Collins *et al.*<sup>6</sup> revealed the fullerene mixing in the polymer matrix of PTB7/PC<sub>71</sub>BM blend film. Due to the low spatial resolution ( $\sim$ several tens of nm) of STXM, however, the domain size had to be enlarged by chemical admixture<sup>6</sup> or thermal annealing at higher temperature<sup>7</sup>. Recently, several experiments revealed sub-structures within the large domains. By means of atomic force microscopy (AFM) coupled with plasma-ashing technique, Hedley *et al.*<sup>8</sup> investigated sub-structure inside the domain (100–200 nm) of PTB7/PC<sub>71</sub>BM blend film prepared without additive and found that the domain consists of a large number of small fullerene spheres (20–60 nm). By means of energy-filtered electron transmission microscopy (EFTEM), Kesave *et al.*<sup>9</sup> reported fiber-like structure,  $\sim 10$  nm wide and  $\sim 100$  nm long, in PGeBTBT/PC<sub>71</sub>BM blend film.

On the other hands, the femtosecond time-resolved spectroscopy is a powerful tool to reveal the carrier formation process within the active layer<sup>10–14</sup>, because the spectroscopy monitors the relative numbers of the photo-created exciton and carrier in the time domain. Significantly, the spectroscopy decouples the carrier formation and transfer processes, because the former process completes within several tens of ps. Actually, the time-resolved spectroscopy revealed that the exciton-to-carrier conversion process in PTB7/PC<sub>71</sub>BM blend film completes within  $\sim 0.3$  ps<sup>10</sup>.

In order to clarify the interrelation between molecular mixing and the photovoltaic properties of BHJ-type OSCs, we selected a liquid-crystalline semiconducting polymer, F8T2, as the donor polymer, because the domain



structure of the blend film with fullerene derivatives remains large (several hundreds of nm) and independent of  $T_{\text{an}}$ <sup>15,16</sup>. Yasuda *et al.*<sup>16</sup> systematically investigated the photovoltaic properties of the OSCs based on films of F8T2/PC<sub>71</sub>BM (33 : 67 wt. %) blend annealed at various temperature ( $T_{\text{an}}$ ): the PCE systematically decreases from the optimal value (=2.28%) at  $T_{\text{an}} = 80^\circ\text{C}$  to 0.81% at  $240^\circ\text{C}$ . Yonezawa *et al.*<sup>17</sup> investigated the charge formation dynamics of F8T2/PC<sub>71</sub>BM blend film by means of the femtosecond time-resolved spectroscopy. Here, we systematically investigated  $T_{\text{an}}$ -dependence of the photovoltaic properties, *i.e.*, short-circuit current ( $J_{\text{sc}}$ ), open-circuit voltage ( $V_{\text{oc}}$ ), fill factor (FF), power conversion efficiency (PCE), internal quantum efficiency ( $\Phi_{\text{IQ}}$ ), charge formation efficiency ( $\Phi_{\text{CF}}$ ), domain size ( $L$ ), and fullerene mixing ( $\Phi_{\text{Fullerene}}$ ) in the polymer matrix in the OSCs based on films of F8T2/PC<sub>71</sub>BM blend.  $\Phi_{\text{CF}}$  is defined by  $n_{\text{formed}}/n_{\text{photon}}$ , where  $n_{\text{formed}}$  and  $n_{\text{photon}}$  are the numbers of the carriers formed at the D/A interface (include weakly bound state) and the absorbed photons, respectively. Absolute value of  $n_{\text{formed}}$  was estimated by combination of the time-resolved and electrochemical spectroscopies.  $\Phi_{\text{CF}}$  is the same as the exciton quenching efficiency, if all the quenched excitons are converted to carriers. We found that  $\Phi_{\text{CF}}$ ,  $\Phi_{\text{IQ}}$ , and PCE are dominantly determined by  $\Phi_{\text{Fullerene}}$ , indicating an essential role of the fullerene mixing in the polymer matrix on the carrier formation and transfer processes.

## Results

**Photovoltaic properties.** First of all, let us survey the device parameter, *i.e.*,  $J_{\text{sc}}$ ,  $V_{\text{oc}}$ , FF, PCE, and  $\Phi_{\text{IQ}}$  against  $T_{\text{an}}$  (Table I). We fabricated OSCs based on films of F8T2/PC<sub>71</sub>BM (33 : 67 wt%) blend annealed for 10 min at  $T_{\text{an}}$  (Fig. S2). We measured current ( $J$ ) – voltage ( $V$ ) curve (Fig. S3) and incident photon-to-current conversion efficiency (IPCE) spectra (Fig. S4). The magnitudes of  $J_{\text{sc}}$  and FF decrease with increase in  $T_{\text{an}}$ , while  $V_{\text{oc}}$  remains nearly independent of  $T_{\text{an}}$ . As a result, PCE ( $=J_{\text{sc}} \times V_{\text{oc}} \times \text{FF}/I_0$ , where  $I_0$  is the power density of the incident light) decreases with increase in  $T_{\text{an}}$ . The  $T_{\text{an}}$ -dependence of  $J_{\text{sc}}$  and FF is ascribed to several compounded factors, *e.g.*, the domain size, carrier recombination process at the D/A interface, and connectivity among the domains. We confirmed that the domain size ( $L$ ) of the active layered is nearly independent of  $T_{\text{an}}$  (*vide infra*).

**Domain structure as investigated by STXM image.** Figure 1 shows STXM images of the F8T2/PC<sub>71</sub>BM blend films annealed at various  $T_{\text{an}}$  probed at 284.4 eV. The photon energy (284.4 eV) was at the  $\pi^*$ -resonance absorption of the fullerene framework<sup>6,18</sup>. Therefore, the bright regions correspond to the fullerene-rich domains, while the dark regions the polymer-rich domains. We performed two-dimensional Fourier transformation to evaluate the length scale ( $L$ ) of the fullerene domain. We regarded the local maxima of the Fourier component as  $L$  (Fig. S5). We found that  $L$  ( $\sim 270$  nm) is nearly independent of  $T_{\text{an}}$ .

**Fullerene mixing as investigated by STXM spectroscopy.** To determine the fullerene mixing, we measured the carbon K-edge absorption spectra ( $\phi_{\text{exp}}$ ) at every 40 nm within the  $2 \mu\text{m} \times 2 \mu\text{m}$  image, *i.e.*,  $50 \times 50$  spectra<sup>19</sup>. We should be careful for evaluation of

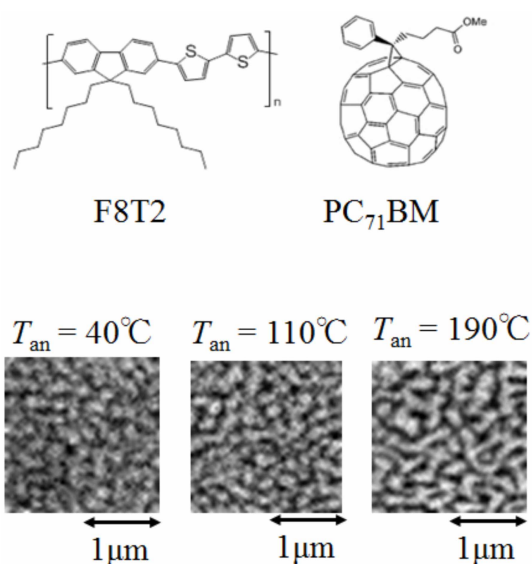


**Figure 1** | STXM image of F8T2/PC<sub>71</sub>BM blend films at 284.4 eV. The bright regions correspond to the PC<sub>71</sub>BM-rich domains, while the dark regions the F8T2-rich domains.

the molecular mixing since the STXM spectra is average along the depth direction. We investigated cross-sectional Plasmon loss image (Fig. S6) of the blend film annealed at  $80^\circ\text{C}$ . We confirmed that the polymer matrix passes completely through to the other side. That is, the fullerene mixing of the polymer matrix is accurately evaluated by the STXM spectroscopy. Unfortunately, we cannot accurately evaluate the molecular mixing of the fullerene domain, because it overlaps with the polymer domain in the depth direction.

Upper panel of Fig. 2 shows the averaged carbon K-edge absorption spectra of the polymer matrix against  $T_{\text{an}}$ . We observed extra bands at both sides of the main peak at 285 eV, as indicated by downward arrows. The bands are ascribed to the 1<sup>st</sup> and 3<sup>rd</sup> peaks of PC<sub>71</sub>BM (see the lower panel of Fig. 2). Their intensities gradually increase with decreases in  $T_{\text{an}}$ , indicating that the fullerene mixing increases with decreases in  $T_{\text{an}}$ . The magnitudes of  $\Phi_{\text{Fullerene}}$  were evaluated by least-squares fitting of the  $\phi_{\text{exp}}$  spectra with the linear combination of the F8T2 ( $\phi_{\text{D}}$ ) and PC<sub>71</sub>BM ( $\phi_{\text{A}}$ ) spectra,  $\phi_{\text{cal}} = C_{\text{D}}\phi_{\text{D}} + C_{\text{A}}\phi_{\text{A}}$ . In the lower panel of Fig. 2, we show an example of the least-squares fitting. The linear combination (black thin curve) well reproduces the overall features of the  $\phi_{\text{exp}}$  spectra. This indicates that the charge-transfer-type absorption at the D/A interface has negligible effects on the  $\phi_{\text{exp}}$  spectra. In the spectral analysis, we select ten  $\phi_{\text{exp}}$  spectra at every  $T_{\text{an}}$  at the central position of the polymer matrix to avoid the artificial mixing of the materials. The averages and standard deviations of  $C_{\text{D}}$  and  $C_{\text{A}}$  were evaluated. The  $\Phi_{\text{Fullerene}}$  values were calculated by  $C_{\text{A}}/(C_{\text{D}} + C_{\text{A}})$ , and are listed in Table II.

**Carrier formation efficiency.** We evaluate the absolute value of  $\Phi_{\text{CF}}$  by combination of the femtosecond time-resolved and

**Table 1** | Device parameters, *i.e.*,  $J_{\text{sc}}$ ,  $V_{\text{oc}}$ , FF, PCE and  $\Phi_{\text{IQ}}$  of OSCs based on films of F8T2/PC<sub>71</sub>BM (33 : 67 wt%) blend annealed for 10 min at  $T_{\text{an}}$ . The error bars of  $J_{\text{sc}}$ ,  $V_{\text{oc}}$ , FF, PCE, and  $\Phi_{\text{IQ}}$  were estimated from standard deviations of more than five OSC devices

$T_{\text{an}}$ ( $^\circ\text{C}$ )	$J_{\text{sc}}$ (mA/cm <sup>2</sup> )	$V_{\text{oc}}$ (V)	FF	PCE (%)	$\Phi_{\text{IQ}}$ @ 400 nm
40	4.37 ± 0.08	0.96 ± 0.01	0.516 ± 0.003	2.17 ± 0.04	0.368 ± 0.011
80	4.17 ± 0.08	0.97 ± 0.01	0.521 ± 0.003	2.12 ± 0.04	0.342 ± 0.009
110	3.96 ± 0.17	0.987 ± 0.006	0.486 ± 0.002	1.92 ± 0.09	0.336 ± 0.009
150	3.68 ± 0.19	0.94 ± 0.02	0.40 ± 0.01	1.37 ± 0.01	0.285 ± 0.007
190	3.51 ± 0.10	0.92 ± 0.01	0.387 ± 0.003	1.25 ± 0.05	0.300 ± 0.010
240	2.94 ± 0.17	0.91 ± 0.01	0.35 ± 0.01	0.95 ± 0.06	0.310 ± 0.015

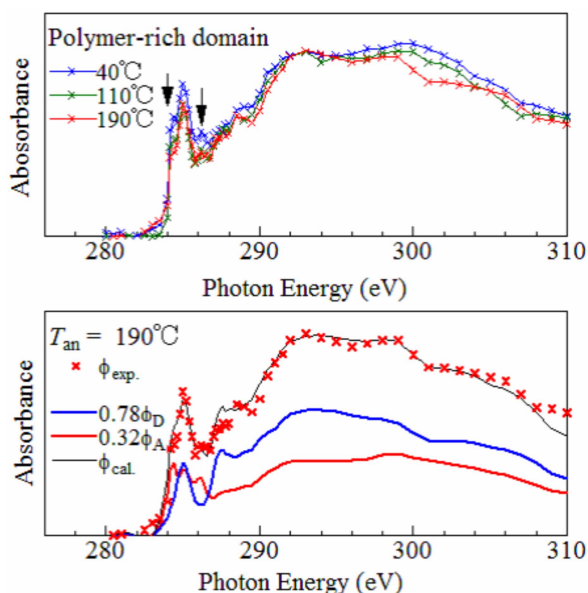


**Figure 2 | Carbon K-edge absorption spectra of the polymer matrix.** Upper panel shows the averaged absorption spectra against  $T_{an}$ . Lower panel shows an example of the spectral decomposition, which was performed by least-squares fitting of the observed spectra ( $\phi_{exp}$ ) with the linear combination of the F8T2 ( $\phi_D$ ) and PC<sub>71</sub>BM ( $\phi_A$ ) spectra,  $\phi_{cal} = C_D\phi_D + C_A\phi_A$ .

electrochemical spectroscopies<sup>20</sup>. Solid curve in Fig. 3 is the differential absorption ( $\Delta OD_{EC}$ ) spectrum of electrochemically oxidized F8T2 neat film. The observed absorption at 1.8 eV is ascribed to the donor carrier. We investigated the spectral intensity ( $I_{1.8eV}$ ) at 1.8 eV against the hole-doping level ( $n$ ) and determined the coefficient ( $\alpha_{carrier} = 4.1 \times 10^{-3} \text{ nm}^2$ ) between  $I_{1.8eV}$  and  $n$  (see Fig. S7). Circles in Fig. 3 is the differential absorption ( $\Delta OD$ ) spectra at 10 ps of the F8T2/PC<sub>71</sub>BM blend film. A sharp photoinduced absorption (PIA) is observed at 1.7 eV, whose profile is similar to that of the  $\Delta OD_{EC}$  spectrum. We confirmed that the spectral profile is unchanged after 10 ps. In addition, the decay time of the PIA is very long ( $\approx 300$  ps). These observations indicate that the PIA is due to the donor carriers. We evaluated the coefficient ( $\alpha_{photon}$ ) between the spectral intensity ( $I_{1.7eV}$ ) at 1.7 eV and the number ( $n_{photon}$ ) of the absorbed photons, with considering the reflection and transmission losses. The  $\Phi_{CF}$  values were calculated by  $\alpha_{photon}/\alpha_{carrier}$ , and are listed in Table II.

**Correlation between parameters.** We summarize in Fig. 4 the interrelation among  $\Phi_{CF}$ ,  $\Phi_{Fullerene}$ ,  $L$ ,  $\Phi_{IQ}$ , and PCE in OSCs against  $T_{an}$ . We note that  $\Phi_{CF}$  has no relation with any losses after

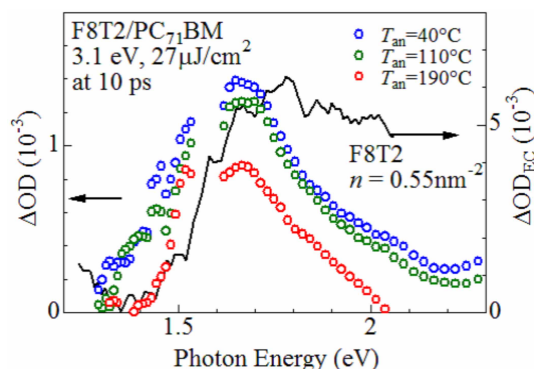


**Figure 3 | Differential absorption ( $\Delta OD$ ) spectra at 10 ps of F8T2/PC<sub>71</sub>BM blend film and differential absorption ( $\Delta OD_{EC}$ ) spectrum of electrochemically oxidized F8T2 neat film.** In  $\Delta OD$ , the excitation photon energy and pulse energy are 3.1 eV and 27  $\mu\text{J}/\text{cm}^2$ , respectively. In  $\Delta OD_{EC}$ , the hole-doping level ( $n$ ) is 0.55  $\text{nm}^{-2}$ .

the carrier formation, e.g., the carrier recombination at the D/A interface or carrier trapping. In this sense,  $\Phi_{CF}$  is easier to interpret than the other efficiencies such as  $\Phi_{IQ}$ , and PCE.  $\Phi_{CF}$  systematically decreases from 0.78 to 0.48 with increase in  $T_{an}$ . In the 2<sup>nd</sup> and 3<sup>rd</sup> panels, we plotted  $\Phi_{Fullerene}$  and  $L$ . The  $T_{an}$  value has no effect on the domain size ( $L \sim 270$  nm), but seems to suppress  $\Phi_{Fullerene}$  in the polymer matrix. The  $T_{an}$ -dependence of  $\Phi_{Fullerene}$ , however, is unclear due to rather large error bars. The error bars come from the bad signal/noise ratio in the featureless spectra. We carefully investigated  $T_{an}$ -dependence of the spectral profile around the fullerene peaks (284–287 eV) in the averaged carbon K-edge absorption spectra. We found that the relative intensities ( $I_{284.4eV}$ ) of the fullerene peak at 284.4 eV systematically decreases with increase in  $T_{an}$  (Fig. S8). This observation indicates that the fullerene mixing in the polymer matrix decreases with increase in  $T_{an}$ . Thus observed  $T_{an}$ -dependence of the fullerene mixing is reasonable, because the thermal annealing at higher  $T_{an}$  accelerates the phase-separation into more pure domains. Our analysis revealed that the fullerene mixing in the polymer matrix is advantageous for the efficient carrier formation. The decrease in  $\Phi_{CF}$  with  $T_{an}$  is responsible for the suppressed  $\Phi_{IQ}$  and PCE (bottom panel of Fig. 4).

## Discussion

To investigate the morphology within the polymer matrix, we investigated cross-sectional TEM-S mapping image of the blend film annealed at 80°C (Fig. S9). The mapping clarifies the distribution of the F8T2 polymer in  $\sim$  nm resolution. The mapping suggests that the F8T2 polymer matrix consists of the polymer clusters of several nm and the fullerene. Such a sub-structure well explains why the F8T2/PC<sub>71</sub>BM OSC shows high  $\Phi_{IQ}$  ( $\approx 0.35$  at 40°C) even though

**Table II | Internal quantum efficiency ( $\Phi_{IQ}$ ), carrier formation efficiency ( $\Phi_{CF}$ ), carrier transfer efficiency ( $\Phi_{CT} = \Phi_{IQ}/\Phi_{CF}$ ), and fullerene mixing ( $\Phi_{Fullerene}$ ) within the polymer matrix of OSCs based on films of F8T2/PC<sub>71</sub>BM (33 : 67 wt%) blend annealed for 10 min at  $T_{an}$ . The error bars of  $\Phi_{CF}$  were roughly evaluated from the signal/noise ratio of the femtosecond time-resolved spectra.  $\Phi_{Fullerene}$  was evaluated by least-squares fitting of the observed spectra ( $\phi_{exp}$ ) with the linear combination of the F8T2 ( $\phi_D$ ) and PC<sub>71</sub>BM ( $\phi_A$ ) spectra,  $\phi_{cal} = C_D\phi_D + C_A\phi_A$ . The averages and standard deviations of  $C_D$  and  $C_A$  were evaluated from ten  $\phi_{exp}$  spectra at every  $T_{an}$ . The  $\Phi_{Fullerene}$  values were calculated by  $C_A/(C_D + C_A)$**

$T_{an}$ (°C)	$\Phi_{IQ}$ @ 400 nm	$\Phi_{CF}$ @ 400 nm	$\Phi_{CT}$ @ 400 nm	$C_D$	$C_A$	$\Phi_{Fullerene}$
40	0.368 ± 0.011	0.76 ± 0.04	0.48 ± 0.04	0.75 ± 0.07	0.47 ± 0.05	0.38 ± 0.08
80	0.342 ± 0.009	0.76 ± 0.04	0.45 ± 0.04	0.85 ± 0.05	0.36 ± 0.06	0.29 ± 0.08
110	0.336 ± 0.009	0.69 ± 0.04	0.49 ± 0.04	0.84 ± 0.04	0.36 ± 0.04	0.30 ± 0.05
150	0.285 ± 0.007	0.53 ± 0.04	0.53 ± 0.05	0.90 ± 0.07	0.33 ± 0.05	0.27 ± 0.07
190	0.300 ± 0.010	0.48 ± 0.04	0.63 ± 0.07	0.76 ± 0.03	0.31 ± 0.06	0.29 ± 0.09
240	0.310 ± 0.015	0.59 ± 0.04	0.53 ± 0.06	—	—	—

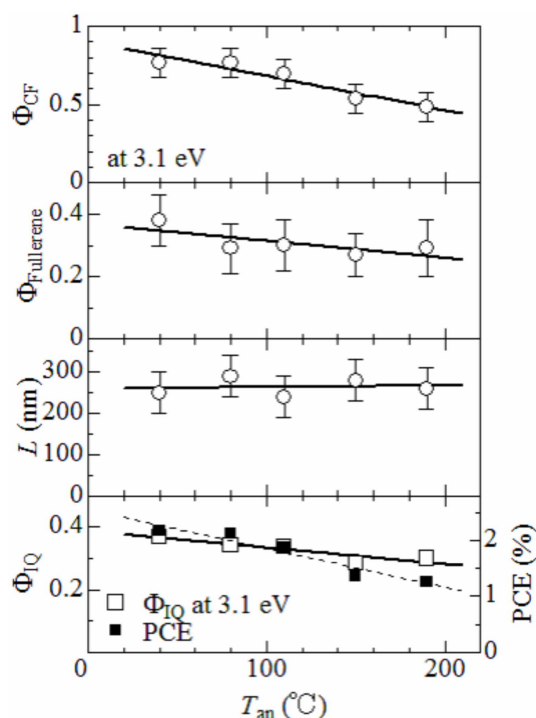


**Figure 4** | Interrelation among  $\Phi_{CF}$ ,  $\Phi_{Fullerene}$ ,  $L$ ,  $\Phi_{IQ}$ , and PCE in OSCs against  $T_{an}$ . Solid straight lines are the results of the least-squares fittings. Error bars of  $\Phi_{IQ}$  and PCE are within the symbol size.

its domain size ( $L \sim 270$  nm) is too large for exciton to reach the domain boundaries. According to this scenario, our observation, *i. e.*,  $\Phi_{CF}$ ,  $\Phi_{IQ}$ , and PCE decreases as the fullerene mixing in the polymer matrix decreases, is interpreted as follows. With increase in  $T_{an}$ , the number (size) of the polymer clusters decreases (increases) within the polymer matrix, because the thermal annealing at higher  $T_{an}$  accelerates the phase-separation into more pure domains in every scale. As a result, the average fullerene concentration ( $\Phi_{Fullerene}$ ) within the polymer matrix decreases with  $T_{an}$ . The decrease in number and the increase in size of the polymer clusters lead to less donor exciton reaching to the D/A interface, to cause the suppressed  $\Phi_{CF}$ ,  $\Phi_{IQ}$ , and PCE. The fullerene mixing is a two-edged blade, because the sub-structure interface also function as recombination point for the photo-generated carriers<sup>21</sup>. Here, we define the carrier transfer efficiency ( $\Phi_{CT}$ ) as  $n_{collected}/n_{formed}$ , where  $n_{collected}$  is the number of the carriers collected as photocurrent (Fig. S1). Then,  $\Phi_{CT}$  is evaluated by  $\Phi_{IQ}/\Phi_{CT}$  (see Table II). We found that  $\Phi_{CT}$  decreases with decrease in  $T_{an}$ . The suppressed  $\Phi_{CT}$  is ascribed to the enhanced carrier recombination process at the sub-structure interface.

## Summary

In summary, we systematically investigated the interrelations between photovoltaic properties,  $\Phi_{CF}$ , and  $\Phi_{Fullerene}$  in OSCs based on films of F8T2/PC<sub>71</sub>BM blend annealed at various  $T_{an}$ . We found that  $\Phi_{CF}$ ,  $\Phi_{IQ}$ , and PCE are dominantly determined by  $\Phi_{Fullerene}$ , not by the size scale ( $L$ ) of the domain. The TEM-S mapping image suggests that F8T2 polymer matrix consist of the polymer clusters of several nm and the fullerene. We interpreted the observation in terms of the polymer clusters within the polymer matrix: the decrease in number and the increase in size of polymer clusters lead to less donor exciton reaching to the D/A interface, to causes of the suppressed  $\Phi_{CF}$ ,  $\Phi_{IQ}$ , and PCE. Even though the stability of the large-scale morphology against  $T_{an}$  is specific to the F8T2/PC<sub>71</sub>BM combination, the annealing effects on the sub-structure are considered to be general to the polymer/fullerene blend film. Thus, complementary study of STXM, which probes quantitative molecular

mixing in several tens of nm scale, and TEM-S mapping, which probes molecular distribution in  $\sim$  nm resolution, is effective to comprehend the photovoltaic properties of OSCs.

## Method

**Synthesis and characterization of the blend film.** F8T2 was purchased from American Dye Source. The weight average molecular weight  $M_w$ , number average molecular weight  $M_n$ , and polydispersity  $M_w/M_n$  were estimated to be 45,000, 13,000, and 3.4, respectively. PC<sub>71</sub>BM (purity 99%) was purchased from Solenne.

For the STXM measurements, F8T2/PC<sub>71</sub>BM blend films were transferred to a Si<sub>3</sub>N<sub>4</sub> membrane. A bilayer film [poly(sodium 4-styrenesulfonate) (PSS)/blend film] was prepared by successive spin-coating of an aqueous solution of PSS and an *o*-dichlorobenzene (*o*-DCB) solution of F8T2/PC<sub>71</sub>BM (33 : 67 wt %). The thicknesses of the as-grown films were 71 nm. The films were annealed for 10 min at  $T_{an} = 40, 80, 110, 150, 190,$  and  $240^\circ\text{C}$  in a N<sub>2</sub> glove box. Then, the bilayer film was cut into  $1 \times 1$  mm<sup>2</sup> pieces, and the substrate was immersed for several minutes in distilled water to etch away the PSS film. Thus, we obtained small F8T2/PC<sub>71</sub>BM films floating on the distilled water. A piece of the floating film was scooped up with the Si<sub>3</sub>N<sub>4</sub> membrane (50 nm in thickness and  $500 \times 500$   $\mu\text{m}^2$  in area).

For the time-resolved spectroscopy, F8T2/PC<sub>71</sub>BM blend films were prepared by spin-coating of an *o*-DCB solution of F8T2/PC<sub>71</sub>BM (33 : 67 wt %) on quartz substrates. The thicknesses of the as-grown films were 60–70 nm. The films were annealed for 10 min at  $T_{an} = 40, 80, 110, 150, 190,$  and  $240^\circ\text{C}$  in a N<sub>2</sub> glove box. The atomic force microscope (AFM) image of the blend film annealed below  $190^\circ\text{C}$  revealed a periodic nanostructure of 300 nm in diameter (Fig. S2). The blend film annealed at  $240^\circ\text{C}$  is known to show macro-scale phase-separation into pure-F8T2 and pure-PC<sub>71</sub>BM domains.

**Fabrication and characterization of the OSC.** The OSCs were fabricated with a structure of indium tin oxide (ITO)/poly(3,4-ethylenedioxythiophene) (PEDOT):PSS (40 nm)/blend film/LiF (1 nm)/Al (80 nm). The patterned ITO (conductivity:  $10 \Omega/\text{square}$ ) glass was pre-cleaned in an ultrasonic bath of acetone and ethanol and then treated in an ultraviolet-ozone chamber. A thin layer (40 nm) of PEDOT:PSS was spin-coated onto the ITO and dried in air at  $110^\circ\text{C}$  for 10 min on a hot plate. The substrate was then transferred to an N<sub>2</sub> glove box and dried again at  $110^\circ\text{C}$  for 10 min on a hot plate. An *o*-DCB solution of F8T2:PC<sub>71</sub>BM (33 : 67 wt %) was subsequently spin-coated onto the PEDOT:PSS surface to form the active layer. The resultant substrates were then annealed at  $T_{an} = 40, 80, 110, 150, 190,$  and  $240^\circ\text{C}$  for 10 min in a N<sub>2</sub> glove box. Finally, LiF (1 nm) and Al (80 nm) were deposited onto the active layer by conventional thermal evaporation at a chamber pressure lower than  $5 \times 10^{-4}$  Pa. The active area of the OSCs is  $2 \times 2$  mm<sup>2</sup>. The  $J$ - $V$  curves (see Fig. S3) were measured using a voltage-current source/monitor under AM 1.5 solar-simulated light irradiation of  $100 \text{ mW}/\text{cm}^2$  (Bunkou-keiki, OTENTO-SUN III). The IPCE spectra (see Fig. S4) was measured using a SM-250 system (Bunkou-keiki). The internal quantum efficiencies ( $\Phi_{IQ}$ ) at 400 nm were estimated with considering the reflection loss.

**STXM spectroscopy and analysis.** The STXM measurement was performed using the compact STXM installed at the BL-13A beamline of the Photon Factory (PF), KEK. The details of the compact STXM are described in the literature<sup>19</sup>. The spatial resolution was 30–40 nm. The carbon K-edge absorption spectra ( $\phi_{exp}$ ) were measured at every 40 nm within the  $2 \mu\text{m} \times 2 \mu\text{m}$  image, *i. e.*,  $50 \times 50$  spectra. The molecular mixing was evaluated by least-squares fitting of the observed spectra ( $\phi_{exp}$ ) with the linear combination of the F8T2 ( $\phi_D$ ) and PC<sub>71</sub>BM ( $\phi_A$ ) spectra,  $\phi_{cal} = C_D\phi_D + C_A\phi_A$ . We regard the absorption spectra of the F8T2 and PC<sub>71</sub>BM domains in the F8T2/PC<sub>71</sub>BM blend film annealed at  $240^\circ\text{C}$  as  $\phi_D$  and  $\phi_A$ , respectively. The coefficients,  $C_A$  and  $C_D$ , are determined so that the evaluation function,

$$F(C_A, C_D) = \sum_i \phi_{exp} (\phi_{exp} - \phi_{cal})^2,$$

becomes the minimum. The background constant component was subtracted so that  $\phi_{cal}$  becomes zero at 280 eV. In the spectral analysis, we select the ten  $\phi_{exp}$  spectra at the central position of the polymer matrix to avoid the artificial mixing of the materials. The averages and standard deviations of  $C_D$  and  $C_A$  were evaluated. The volume fractions of fullerene ( $\Phi_{Fullerene}$ ) were calculated by  $C_A/(C_D + C_A)$ .

**Femtosecond time-resolved spectroscopy.** The time-resolved spectroscopy was performed in a pump-probe configuration. In order to reduce the irradiation damage, the blend films were placed in N<sub>2</sub> atmosphere. The pump pulse at 400 nm was generated as the second harmonics of a regenerative amplified Ti:sapphire laser in a  $\beta$ -BaB<sub>2</sub>O<sub>4</sub> (BBO) crystal. The pulse width, repetition rate, and pulse energy were 100 fs, 1000 Hz, and 27  $\mu\text{J}/\text{cm}^2$  respectively. The frequency of the pump pulse was decreased by half (500 Hz) to provide “pump-on” and “pump-off” conditions. A white probe pulse (500–900 nm), generated by self-phase modulation in a sapphire plate was focused on the sample with the pump pulse. The spot sizes of the pump and probe pulses were 4.0 and 2.0 mm in diameter, respectively. The differential absorption ( $\Delta OD$ ) spectrum is expressed as  $-\log(I_{on}/I_{off})$ , where  $I_{on}$  and  $I_{off}$  are the transmission spectra under the pump-on and pump-off conditions, respectively.

**Electrochemical spectroscopy.** The electrochemical spectroscopy was carried out in an optical two-pole cell with a pair of quartz windows. The electrochemical hole-



doping was performed against Li metal in propylene carbonate (PC) solution containing 1 mol/L LiClO<sub>4</sub>. The F8T2 neat film was spin-coated on an ITO glass substrate from *o*-DCB solution, and was dried in a N<sub>2</sub> glove box. The thicknesses was 67 nm. The active area of the film was 2.25 cm<sup>2</sup>, and the reduction current was 100 nA. The voltage in the hole-doping process were 3.8 V vs. Li. The differential absorption ( $\Delta OD_{EC}$ ) spectrum of electrochemically oxidized film is expressed as  $-\log(I_{doped}/I_{non})$ , where  $I_{doped}$  and  $I_{non}$  are the transmission spectra of the hole-doped and non-doped films, respectively.

The charge formation efficiency ( $\Phi_{CF}$ ) was determined by combination of the time-resolved and electrochemical spectroscopies<sup>20</sup>. The former spectroscopy tells us the coefficient ( $\alpha_{\text{photon}}$ ) between  $\Delta OD$  and  $n_{\text{photon}}$ , while the latter spectroscopy tells us the coefficient ( $\alpha_{\text{carrier}}$ ) between  $\Delta OD_{EC}$  and  $n$ . Then, the  $\Phi_{CF}$  value is calculated by  $\alpha_{\text{photon}}/\alpha_{\text{carrier}}$ .

- Hiramoto, M., Fujiwara, H. & Yokoyama, M. Three-layered organic solar cell with a photoactive interlayer of codeposited pigments. *Appl. Phys. Lett.* **58**, 1062–1064 (1991).
- Sariciftci, N. S., Smilowitz, L., Heeger, A. J. & Wudl, F. Photoinduced electron transfer from a conducting polymer to buckminsterfullerene. *Science* **285**, 1474–1476 (1992).
- Nguyen, T. L. *et al.* Semi-crystalline photovoltaic polymers with efficiency exceeding 9% in a  $\sim 300$  nm thick conventional single-cell device. *Energy Environ. Sci.* **7**, 3040–3051 (2014).
- Guo, X. *et al.* Enhanced photovoltaic performance by modulating surface composition in bulk heterojunction polymer solar cells based on PBDTTT-C-T/PC<sub>71</sub> BM. *Adv. Mater.* **26**, 4043–4049 (2014).
- He, Z. *et al.* Enhanced power-conversion efficiency in polymer solar cells using an inverted device structure. *Nature Photon.* **6**, 591–595 (2012).
- Collins, B. A. *et al.* Absolute measurement of domain composition and nanoscale size distribution Explains Performance in PTB7:PC<sub>71</sub>BM solar cells. *Adv. Energy Mater.* **3**, 65–74 (2013).
- Ma, W. *et al.* Domain purity, miscibility, and molecular orientation at donor/acceptor interfaces in high performance organic solar cells: paths to further improvement. *Adv. Energy Mater.* **3**, 864–872 (2013).
- Hedley, G. J. *et al.* Determining the optimum morphology in high-performance polymer-fullerene organic photovoltaic cells. *Nature Commun.* **4**, 2867 (2013).
- Kesava, S. V. *et al.* Domain composition and fullerene aggregation govern charge photogeneration in polymer/fullerene solar cells. *Adv. Energy Mater.* **4**, 1400116 (2014).
- Yonezawa, K., Kamioka, H., Yasuda, T., Han, L. & Moritomo, Y. Fast carrier formation from acceptor exciton in low-gap organic photovoltaic. *Appl. Phys. Express* **5**, 042302 (2012).
- Guo, J. *et al.* Structure, dynamics, and power conversion efficiency correlations in a new low bandgap polymer: PCBM solar cell. *J. Phys. Chem. B* **114**, 742–748 (2010).
- Hwang, I.-W., Moses, D. & Heeger, A. J. Photoinduced carrier generation in P3HT/PCBM bulk heterojunction materials. *J. Phys. Chem. C* **112**, 4350–4354 (2008).
- Guo, J., Ohkita, H., Benten, H. & Ito, S. Charge generation and recombination dynamics in Poly(3-hexylthiophene)/fullerene blend films with different regioregularities and morphologies. *J. Am. Chem. Soc.* **132**, 6154–6164 (2010).
- Marsh, R. A., Hodgkiss, J. M., Albert-Seifried, S. & Friend, R. H. Effect of annealing on P3HT:PCBM charge transfer and nanoscale morphology probed by ultrafast spectroscopy. *Nano Lett.* **10**, 923–930 (2010).

- Huang, J.-H. *et al.* Enhanced spectral response in polymer bulk heterojunction solar cells by using active materials with complementary spectra. *Sol. Energy Mater. Sol. Cells* **94**, 22–28 (2010).
- Yasuda, T. *et al.* Photovoltaic properties and charge dynamics in nanophase-separated F8T2/PCBM blend films. *J. Photopolym. Sci. Technol.* **25**, 271–276 (2012).
- Yonezawa, K. *et al.* Charge-transfer state and charge dynamics in poly(9,9'-dioctylfluorene-co-bithiophene) and [6, 6]-phenyl C<sub>70</sub>-butyric acid methyl ester blend film. *Appl. Phys. Express* **4**, 122601 (2011).
- Moritomo, Y. *et al.* Molecular mixing in donor and acceptor domains as investigated by scanning transmission X-ray microscopy. *Appl. Phys. Express* **7**, 052302 (2014).
- Takeichi, Y., Inami, N., Suga, H., Ono, K. & Takahashi, Y. Development of a compact scanning transmission X-ray microscope (STXM) at the photon factory. *Chem. Lett.* **43**, 373–375 (2014).
- Moritomo, Y., Yonezawa, K. & Yasuda, T. Effect of temperature on carrier formation efficiency in organic photovoltaic cells. *Appl. Phys. Lett.* **105**, 073902 (2014).
- Dimitov, S. D. & Durrant, J. R. Materials design consideration for charge generation in organic solar cells. *Chem. Mater.* **26**, 616–630 (2014).

## Acknowledgments

This work was partially supported by a Grant-in-Aid (No. 23684022) for Scientific Research from the Ministry of Education, Culture, Sports, Science and Technology, Japan. The STXM measurements were performed under the approval of the Photon Factory Program Advisory Committee (Proposal No. 2013S2-003). We thank Dr. K. Yase of AIST for his helpful advice on the fabrication of the STXM samples.

## Author contributions

Y.M. and T.Y. planned the overall the experiment. Y.M. analyzed the STXM spectra and wrote the main manuscript. T.Y. fabricated and characterized the organic solar cells. K.Y. performed time-resolved and experiment spectroscopies and their analyses. T.S. contribute the analyses of the X-ray absorption spectra. Y.T., H.S., Y.T., N.I., K.M. and K.O. construct and operated the STXM machine.

## Additional information

Supplementary information accompanies this paper at <http://www.nature.com/scientificreports>

**Competing financial interests:** The authors declare no competing financial interests.

**How to cite this article:** Moritomo, Y. *et al.* Fullerene mixing effect on carrier formation in bulk-hetero organic solar cell. *Sci. Rep.* **5**, 9483; DOI:10.1038/srep09483 (2015).



This work is licensed under a Creative Commons Attribution 4.0 International License. The images or other third party material in this article are included in the article's Creative Commons license, unless indicated otherwise in the credit line; if the material is not included under the Creative Commons license, users will need to obtain permission from the license holder in order to reproduce the material. To view a copy of this license, visit <http://creativecommons.org/licenses/by/4.0/>